Continental Shelf Research 124 (2016) 49–62

Contents lists available at ScienceDirect

Continental Shelf Research

journal homepage: www.elsevier.com/locate/csr

Research papers

An assessment of transport timescales and return coefficient in adjacent tropical estuaries

Fernando P. Andutta [a,b,*], Fernanda Helfer [a], Luiz Bruner de Miranda [b], Eric Deleersnijder [c,d], Christopher Thomas [e], Charles Lemckert [a]

[a] Griffith School of Engineering and Griffith Change Response Program (GCCRP), Griffith University, Gold Coast, QLD 4222, Australia
[b] Oceanographic Institute, University of São Paulo, São Paulo CEP 05508-900, Brazil
[c] Université catholique de Louvain (UCL), Institute of Mechanics, Materials and Civil Engineering (IMMC) & Earth and Life Institute (ELI), 4 Avenue Georges Lemaître, Bte L4.05.02, B-1348 Louvain-la-Neuve, Belgium
[d] Delft University of Technology, Delft Institute of Applied Mathematics (DIAM), Mekelweg 4, 2628CD Delft, The Netherlands
[e] Université catholique de Louvain (UCL), Institute of Mechanics, Materials and Civil Engineering (IMMC), 4 Avenue Georges Lemaître, Bte L4.05.02, B-1348 Louvain-la-Neuve, Belgium

ARTICLE INFO

Article history:
Received 5 November 2015
Received in revised form
8 May 2016
Accepted 11 May 2016
Available online 12 May 2016

Keywords:
Tropical estuary
Residence time
Exposure time
Return coefficient
Numerical model
Hydrodynamics

ABSTRACT

Transport timescales (TTS), namely residence time and exposure time, were computed for adjacent shallow meso-tidal tropical estuarines system using the Lagrangian model D-Waq Part coupled with the hydrodynamic model Delft3D-Flow, and the Constituent-oriented Age and Residence time Theory, CART. The main results are threefold: (a) The TTS differs more between releases at high or low tide than between those at spring and neap tides. The exposure time was also calculated and found to be larger than the residence time by a few days. (b) The exposure and residence times were used to evaluate the return coefficient (r) for different scenarios. As with residence and exposure times, the return coefficient was found to differ more between releases at high or low tide than between those at spring and neap tides. (c) For the Caravelas Estuary, where the river inflow was low ($\sim 4\ m^3\ s^{-1}$), the residence time was found to be much larger than for the Peruípe Estuary, where the river discharge was greater and nearly constant during the sampling period ($\sim 20\ m^3\ s^{-1}$). These results shows the importance of advection in decreasing TTS in the Peruípe Estuary compared to the Caravelas Estuary. The influence of the advection and dispersion agrees with previous simple estimates obtained using the newly modified Land Ocean Interaction Coastal Zone (LOICZ) model by Andutta et al. (2014).

1. Introduction

Since the dynamics of most estuarine systems is relatively complex, studies of transport timescales (TTS) provide valuable insight into estuarine behaviour. Transport timescales represent a more holistic way of interpreting the flow in complex systems (e.g. Monsen et al., 2002), and allow us to understand how advective and dispersive mechanisms transport water.

Transport timescales are driven by the water currents, which in turn are influenced by sea level oscillation, bathymetry and the temperature and salinity fields. It is therefore necessary to have an accurate representation of these quantities in order to satisfactorily estimate transport timescales.

This article has the following tasks:

(1) to demonstrate, using a 3D hydrodynamic model combined with particle simulations, how release times (e.g. slack waters of high and low tides, neap and spring tides) affect the exposure time and residence time in a shallow meso-tidal tropical estuary.
(2) to compare TTS results from numerical modelling with estimates using the simple newly modified Land Ocean Interaction Coastal Zone (LOICZ) model by Andutta et al. (2014).
(3) to calculate and evaluate the return coefficient (r) numerically and analytically using CART. This is a measure of the propensity of a water parcel to return into the domain of interest after leaving it.

1.1. Overview of transport timescales

Since the pioneering work by Ketchum (1951) and Bolin and Rodhe (1973), the theory of TTS has evolved (e.g. CART, www.climate.be/cart), and other TTS definitions have been introduced in order to fill scientific gaps. Therefore, there are many different

* Corresponding author at: Griffith School of Engineering, Griffith University, Gold Coast, QLD 4222, Australia.

http://dx.doi.org/10.1016/j.csr.2016.05.006
0278-4343/

transport timescale definitions, e.g. flushing time (Ketchum, 1951; Fischer et al., 1979; Monsen et al., 2002), residence time (Bolin and Rodhe, 1973; Monsen et al., 2002; Delhez et al., 2004; Deleersnijder et al., 2006), exposure time (Monsen et al., 2002), transit time (Holzer and Hall, 2000), influence time (Delhez et al., 2014), age (Bolin and Rodhe, 1973; Monsen et al., 2002), e-folding flushing time (Monsen et al., 2002), turnover time (Sheldon and Alber, 2006) and renewal time (Andutta et al., 2014) – all of which have their own interpretation.

Two timescales, residence time and exposure time, are used to provide an indication of increase or decrease of non-reactive and reactive substances in estuaries, bays, lagoons, and atolls (Andutta et al., 2014). The residence time (Θ) is the time needed for a particle constituent to reach for the first time an open boundary of the domain of interest (e.g. Delhez et al., 2004). The exposure time (φ) is the time the particle will stay in the domain (e.g. Monsen et al., 2002) (Fig. 2). Therefore, at a given time and location, the exposure time is always larger than or equal to the residence time. The larger the difference between the two timescales, the more often the particles tend to re-enter the domain of interest after leaving it for the first time. To evaluate the exposure time, the computational domain must be larger than the domain of interest (de Brauwere et al., 2011; de Brye et al., 2012). Estimates of these timescales may be obtained in an Eulerian or a Lagrangian framework. The latter often requires sufficiently large number of numerical particles in order to provide a result that statistically approaches the real condition.

A dimensionless return coefficient, r, represents the propensity of particles to return into the estuary after reaching an open boundary for the first time, as illustrated in Fig. 1A (de Brauwere et al., 2011). It is defined as the relative difference between φ and Θ, i.e.

$$r = \frac{(\Theta - \varphi)}{\Theta}. \quad (1)$$

Clearly, this coefficient lies in the interval [0,1].

The larger the r the more likely it is that particles will re-enter the estuary after crossing one of its open boundaries for the first time. Accordingly, particles that never return into the estuary have $r=0$, while particles returning often or for long periods of time have r close to unity.

1.2. Chosen estuary and coastal area

The domain of interest is the estuarine System of the Caravelas and Peruípe Rivers (ESCP), in southern Bahia state, Brazil (see Fig. 2); more details may be found in Appendix 1. It is located at the approximate latitude of 17°50′S, nearly 60 km from the National Maritime Park of Abrolhos, which is one of the largest reef structures of the Atlantic ocean, providing habitat for innumerous marine species. The ESCP has two main mouths: the Caravelas Estuary in the north (17°45′S), with two small channels named Barra Velha (~1 km wide) and Tomba's Mouth (~600 m wide), and the Peruípe Estuary in the south (17°54′S) with a funnel shape ranging in width from ~3500 m to ~700 m in the first few hundred meters. These two mouths are separated by a distance of ~25 km alongshore, and are internally connected by shallow and narrow channels around Cassurubá or Cassumba Island. Our simulations consider the domain shown in Fig. 1C, for which results were computed according to the number of particles in the control domain with boundaries ω_1 and ω_2.

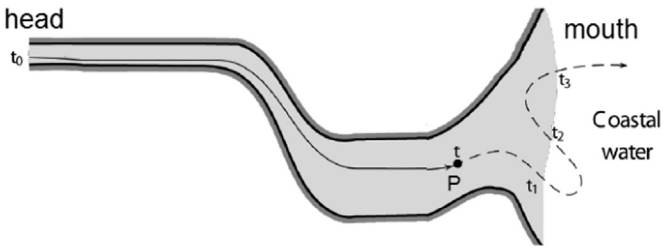

Fig. 1. Path of a particle in the estuary from the upstream boundary (head) to the downstream boundary (mouth). For a particle initially at position P at time t, the residence time is t_1–t, the exposure time is $(t_3–t_2) + (t_1–t)$.

2. Methods

2.1. Numerical model

The ESCP comprises a number of channels varying significantly in width, from 60 m upstream to 1000 m near the mouth, and thus a high resolution mesh is necessary to resolve the many small channels in the domain. The numerical model used is the curvilinear-mesh, three-dimensional Delft3D-Flow from Deltares (www.deltares.nl). This model is hydrostatic, and its equations are solved by the method of finite differences (Delft Hydraulics, 2008). A curvilinear mesh is appropriate for the domain, although there are some disadvantages in the horizontal resolution distribution compared to unstructured meshes. Delft3D's curvilinear mesh is efficient in minimizing noise due to the steps in the horizontal plane, and allows the mesh cells to follow the channels more easily compared to non-curvilinear quadrangular meshes. The degree of non-orthogonality between mesh elements is always smaller than 0.02 thus satisfying the criteria ($\cos\pm < 0.02$), which helps to preserve numerical stability of the simulations (Delft Hydraulics, 2008). The diagonal horizontal resolution ranges from ~20 m to ~300 m. The number of quadrangular mesh cells on the horizontal plane is 22,928. A lower resolution is applied in the coastal region ~[130–300] m, but this is increased toward the coast and the estuary ~[20–100] m (Fig. 1B). The refined mesh within the estuary combined with high water speeds requires the time-step to be relatively small (around 1 s), to satisfy the Courant–Friedrichs–Lewy condition. The mesh used in the simulations of the ESCP (Fig. 1B) is relatively complex, covering a small part of the Peruípe River, near the city of Nova Viçosa. This river is the main channel connecting the northern and southern mouths. The main tributaries of the Caravelas River, namely the Cupído and Jaburuna Rivers, are covered by the mesh. With 10 equally spaced sigma vertical layers, this mesh also covers a few kilometers of the adjacent coastal region.

The bathymetry in the estuarine channels was obtained using an Echo sounder and Global Position System. Two tide gauges were installed in Caravelas and Nova Viçosa (see locations A and C in Fig. 2), meant to remove the tides from the Echo sounder data. For the Peruípe River estuary, the bathymetry was measured only in the first 6 km, near anchor station D. Thus an extrapolation was applied, considering the depth to be 4 m for the next 14 km along the Peruípe River. The bathymetry was combined from these sources, and the triangular interpolation application in Delft3D-Flow was used. The bottom topography has depths ranging from ~0.2 m to a maximum of ~18 m (Tomba's Mouth), whilst in the coastal region do not exceed ~10 m.

A more detailed description of the field work carried out to obtain measurements of thermohaline properties and other parameters is provided in Appendix 2.

2.2. Model boundary conditions, initial conditions and physical parameters

Rainfall and river discharge measurements in the Peruípe River are shown in Fig. 3B. The river discharge data, obtained from the

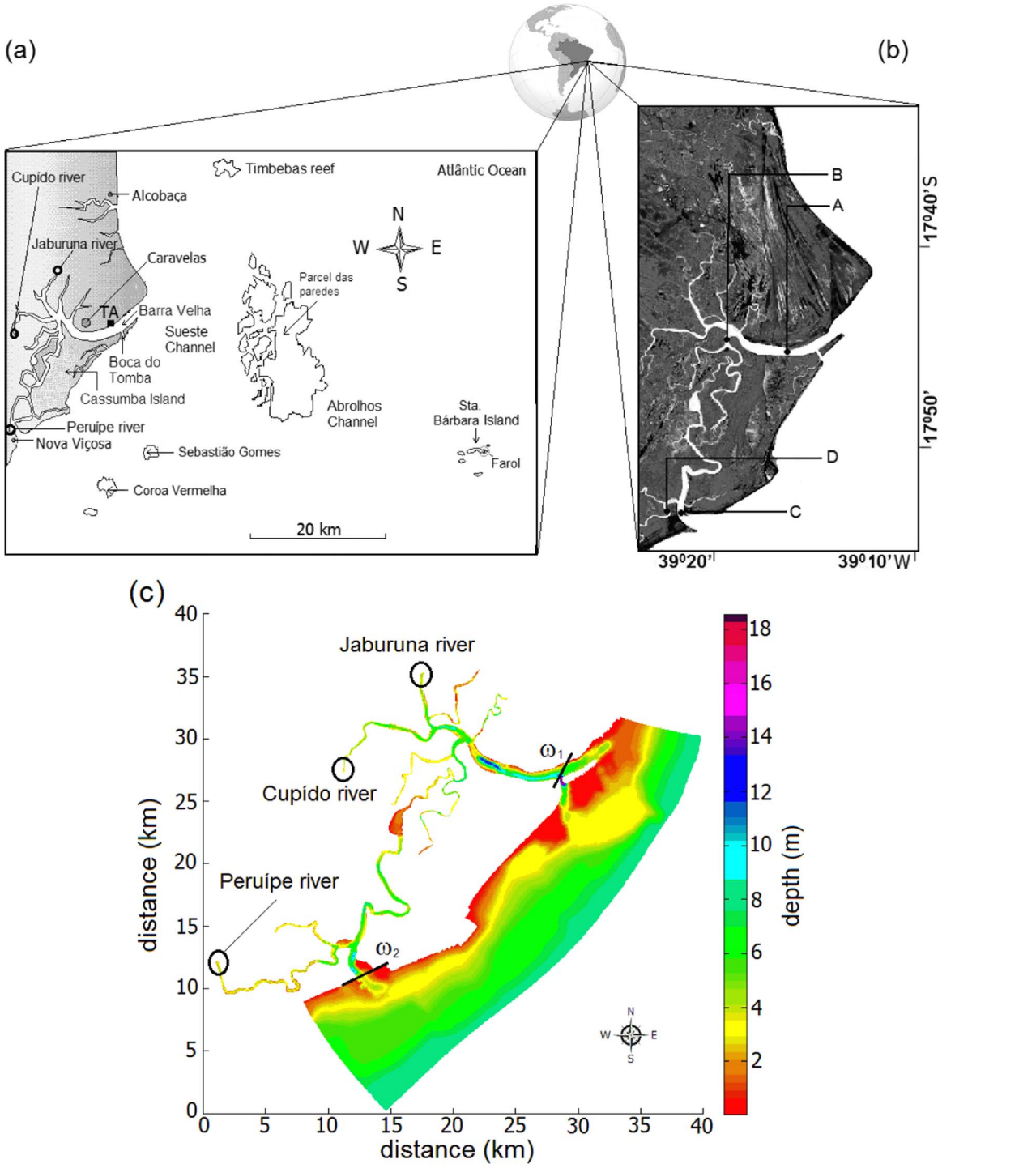

Fig. 2. (a) Geographic location of the estuarine system comprising the Caravelas and Peruípe rivers. Aracruz terminal harbour – TA, and the Sueste and Abrolhos channels, the Parcel das paredes and the National Marine Park of Abrolhos. (b) Detailed image of the estuarine system, and location of the oceanographic mooring sites A and B in Caravelas area, and C and D in Nova Viçosa area, where D is referred as site E at Andutta et al., 2013. (c) numerical domain with ω_1 and ω_2 denoting the limit of the control domain ω to compute the transport timescales.

National Agency of Waters ANA (http://www.ana.gov.br/), was measured at a gauge station upstream of the river, at station Helvécia no. 55510000 (code 1739006). This station covers a large part of the drainage basin of the river. During rainy conditions the total drainage basin of the river may be used to estimate the total river flow to be applied at the upstream inflow boundary of the river. The factor to account for the missing drainage basin area is $\alpha = \frac{A_1+A_2}{A_1} = 1.6$, in which station Helvécia $A_1 \sim 2840\ \text{km}^2$, and the downstream area not covered by this gauge station is $A_2 \approx 1760\ \text{km}^2$. The area values were obtained from the ANA (http://hidroweb.ana.gov.br/).

Data from the gauge station were also used to estimate the river discharge range for the Cupído and Jaburuna rivers. This was done by comparing their watershed areas with the watershed of the Peruípe river, and assuming homogeneous rainfall and evapotranspiration distributions over these areas (Andutta, 2011; Pereira et al., 2010). The total river flow into Caravelas Estuary was

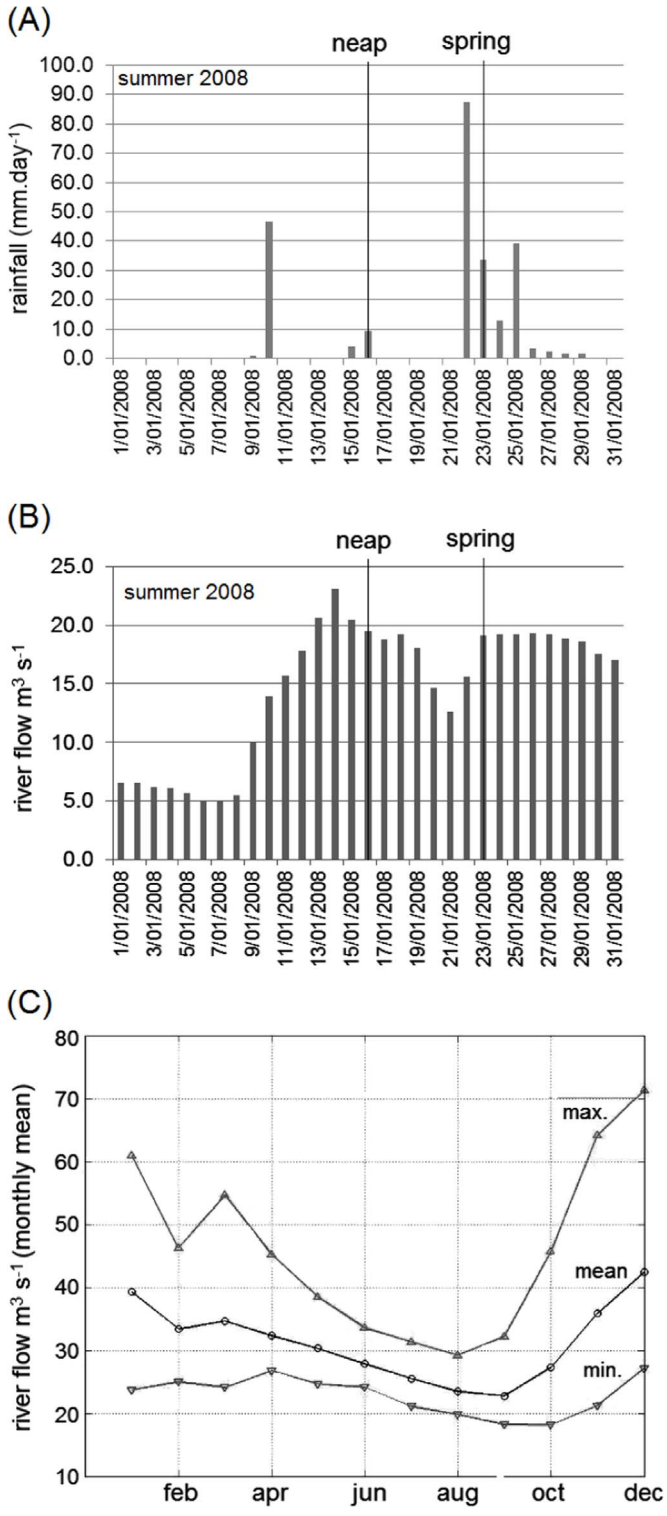

Fig. 3. Daily variation of the rainfall (A), and river dischage (B) during January (2008), observations were made at the gauge station Helvécia no. 55510000 (código 1739006) – National Agency of Waters. (C) Climatological estimate of the mean, minimum (min.) and maximum (max.) monthly river dischage using data from 1975 to 2008 (34 years of measured river flow) and corrected using the factor 1.6 to account for the entire drainage basin area of the Peruípe River.

then roughly estimated using $\pm$, where $\beta = 600/4600$ is the ratio between the catchment areas of the Caravelas (600 km^2) and the Peruípe ($A_1+A_2=4600$ km^2) rivers, and Q_P is the average discharge for the Peruípe). This estimation was adjusted by comparing observed flow velocities at locations A and B with model predictions.

Table 1.
Summary of flow conditions in the simulations for the Peruípe, Cupído, and Jaburuna rivers. Data from ANA.

River	Flow ($m^3 s^{-1}$) January 2008	Typical range of flow ($m^3 s^{-1}$) in wet season	Salinity applied to boundary cells
Peruípe	~5–20	17–70	0
Cupído	2	2–9	6
Jaburuna	2		4

The monthly estimate of fresh water inflow for the Peruípe River reveals small inflow for the dry season, often between June and September (see Fig. 3C). The combined freshwater input from the Jaburuna and Cupído rivers estimated using the factor β is less than 10% of the river discharge into the Peruípe River. Because the field work was conducted during a relatively dry wet season, when rainfall was negligible prior to and during measurements obtained in January 2008 (Fig. 3A), it is logical not to consider the application of the factor α at the Helvécia gauge station. Although this approach of river flow estimation is not required, the technique described above would be required under homogeneous rainfall conditions over the drainage basin of the Peruípe, Jaburuna and Cupído rivers.

The best fit between observations and model results was obtained using the mean river discharge shown in Table 1 for the Cupído and Jaburuna rivers, and the daily measurements shown in Fig. 3B for the Peruípe River. In other words, the value measured at Helvécia gauge station was used in the simulation with additional tuning to extrapolate results for the other two smaller rivers.

The measurements from this tide gauge were compared with the simulation results during neap and spring tides using the "Skill" method described below. In addition, a qualitative comparison was carried out between the axial salinity distribution found in the simulations, and the observed distribution presented in Schettini and Miranda (2010).

We used the initial condition of a homogeneous thermohaline distribution for the salinity (30 practical salinity unit – psu) and temperature (27 °C). The spin up simulation was made for about two months to obtain a dynamic equilibrium condition. Since the temperature has previously been found to be nearly homogeneous in this estuary (Andutta, 2011), its mean value was used for all simulations. The first flow field and salinity distribution, obtained

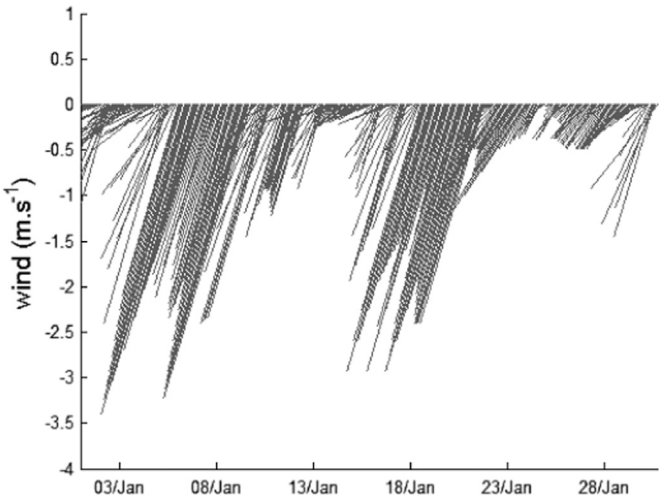

Fig. 4. Wind data obtained from the Instituto National de Meteorologia INMET. Data during January 2008 at Caravelas station, code INMET A405, and coordinates (Lat. 17°43′48.0″S; Long. 39°15′00.0″W).

Table 2.
Amplitude and frequency of the main tidal components recorded at Terminal Aracruz – TA.

Component	Amplitude (cm)	Frequency (deg. h^{-1})
O_1	8.89	13.94
K_1	5.76	15.04
P_1	1.91	14.96
Q_1	1.62	13.40
M_2	75.10	28.98
S_2	33.48	30.00
L_2	15.06	29.53
N_2	13.45	28.44
K_2	9.11	30.08

Table 3.
Sensitivity analysis of the salinity to the value of the horizontal diffusivity K_h using the Skill method from Wilmott (1981). Skill values are in the range 0–1. The factor f was used in the sensitivity analyses following formulae by Okubo (1971).

Parameter	Site A (Skill)	Site B (Skill)	Site C (Skill)	Site D (Skill)
***f* =2**				
Salinity (neap)	0.78	0.58	0.55	0.70
Salinity (spring)	0.85	0.62	0.60	0.75
***f* =100**				
Salinity (neap)	0.86	0.72	0.68	0.74
Salinity (spring)	0.90	0.76	0.75	0.82
***f* =150**				
Salinity (neap)	0.80	0.76	0.64	0.72
Salinity (spring)	0.95	0.80	0.80	0.88
***f* = 200**				
Salinity (neap)	0.85	0.80	0.73	0.78
Salinity (spring)	0.97	0.85	0.83	0.93
***f* =250**				
Salinity (neap)	0.81	0.77	0.72	0.74
Salinity (spring)	0.94	0.81	0.78	0.89
***f* =400**				
Salinity (neap)	0.81	0.74	0.66	0.65
Salinity (spring)	0.85	0.78	0.70	0.79
***f* =2000**				
Salinity (neap)	0.64	0.56	0.50	0.60
Salinity (spring)	0.66	0.60	0.54	0.65

from the equilibrium condition, was used to provide a varied initial field for simulations starting at slack waters in both spring and neap tidal conditions.

Computational modellers often assume that vertical eddy diffusion and viscosity coefficients vary in time, by using turbulent closure models, e.g. algebraic, *k-L*, *k-Epsilon* schemes. On the other hand, the horizontal eddy diffusivity, K_h, and horizontal viscosity coefficients, K_v, are often estimated according to the mesh element size (Okubo, 1971). Therefore, modellers need to choose a parameterisation scheme that provides the right amount of mixing in the estuary. We have considered the parameterisation of horizontal eddy viscosity by Uittenbogaard et al. (1992), which is available in Delft3D-Flow and reproduces well the turbulent fluxes of momentum.

The best fit between results and simulations was obtained assuming the horizontal eddy diffusivity, K_h, to be in the range of $\sim$[2–30] $m^2\ s^{-1}$ with small and large values applied respectively to small and large mesh cells. The sensitivity analysis for K_h, was conducted following Okubo (1971). Because Okubo's formula applies for open-water, it was observed that it was not properly simulating the true dispersion in the estuary, thus a factor f was used to increase and decrease mixing at the sub-grid scale (See Eq. (2)). Varying f allowed us to achieve the best fit between measurements and model results.

$$K_h = f\left[2.05 \times 10^{-4} x\ d^{1.15}\right] \quad (2)$$

where d is the mesh cell size (from $\sim$20 to $\sim$300 m), and f is the factor set to different values but only shown for 2, 100, 150, 200, 250, 400 and 2000 in the sensitivity analyses (see Table 3).

The *k-Epsilon* turbulent closure scheme was used to compute values for the vertical viscosity and diffusivity. We assumed the typical Manning roughness coefficient of ($0.02\ m^{-1/3}$ s), which characterises the higher percentage of local sediment (Sousa et al., 2012). This resulted in a Chézy coefficient of $\sim$40 $m^{-1/2}$/s. Wind speed and directions, assumed to be constant over this small region, were obtained at the Caravelas station from the Instituto Nacional de Meteorologia INMET (code INMET 86764), at (source: http://www.inmet.gov.br/portal/), see Fig. 4.

The wind was assumed to only affect mesh cells in coastal areas. In other words, the wind stress did not affect mesh cells inside the estuarine channels. Moreover, Andutta et al. (2013) applied Hansen and Rattray's analytical equation of the velocity and salinity components, and demonstrated that the wind effect in January 2008 was negligible at station C (near Nova Viçosa estuarine mouth), which is the closest to the coast. Hansen and Rattray's analytical solution required an adjustment of no more than 0.02 Pa for the wind stress, which correspond to wind speeds of $\sim$ 3 m s^{-1} (Andutta et al., 2013). South-southwestward alongshore currents occur between October and January, while north-northeastward alongshore currents are observed during the fall and winter months Lessa and Cirano (2006).

Sea level data from TOPEX were used to force tides at the open boundary nodes. A time series of water surface elevation from May to July 2007 was recorded at Terminal Aracruz (TA in Fig. 2), which is a few kilometers away from the coastal open boundary. At TA a total of 16,264 tidal measurements were recorded at five minute intervals, and were processed using the tidal component extraction program PACMARÉ (Franco, 2000). These tidal measurements were used to obtain the amplitude and phase of the main tidal components, shown in Table 2. Additionally, sea-level data were recorded at stations A and C from 14th to 19th of January 2008, and these data were used to validate modelled sea-level oscillation (comparison shown in Results and Discussion section). Sea surface elevation observations from sites A and C showed the same phase, strongly suggesting that tides propagate across the shelf, because tides propagating along the coast would results in a phase shift between sea level observations at sites A and C (see Fig. 2). The measurements of tidal heights of $\sim$1 m and $\sim$3 m during neap and spring tides, respectively. This ranks as meso-tidal, according to the criteria of Davies (1974) for tidal classification. From the tidal heights shown in Table 3, the tidal form-number is [$N_f=(K_1+O_1)/(M_2+S_2)=0.19$], indicating a semidiurnal tidal estuary (Defant, 1960). The tidal components from Table 2 represent over 97% of sea level variations for the estuarine system (Andutta, 2011).

2.3. Model validation criteria

In order to quantify the agreement between the simulated velocity and salinity profiles the method suggested by Wilmott (1981), based on the Skill parameter was used. Accordingly, the skill is measured as follows:

$$Skill = 1 - \frac{\Sigma |X_{\mathrm{mod}} - X_{obs}|^2}{\Sigma \left(|X_{\mathrm{mod}} - \overline{X}_{obs}| + |X_{obs} - \overline{X}_{obs}|\right)^2}, \quad (3)$$

where X_{obs} and X_{model} denote the observational and simulated properties, respectively, $\overline{X}_{obs}$ being the mean observational values. The Skill parameter varies from 1 to zero, with 1 indicating the best fit, and zero indicating a complete disagreement between observation and model results.

2.4. Modelling approach to calculate the transport timescales

To quantify the residence time and exposure time 35 thousand numerical particles were released in the estuary by coupling D-Waq PART with results from the Delft3D-FLOW(i.e. within the subdomain denoted ω). Numerical particles were deployed near the bottom and top layers. The particle concentration using conservative tracer module was normalised to value 1 within the volume of ω. Therefore, the number of particles decreases when particles exit ω, and increases when particles re-enter ω. The minimal initial number of particles, i.e. 25 thousand, was computed considering a minimum thickness of 2 m and a grid cell of ~20 by 10 m.

A total of four simulation scenarios were made: (S_1) particle released at high water in neap tide, (S_2) particle released at low water in neap tide, (S_3) particle released at high water in spring tide, and (S_4) particle released at low water in spring tide.

In order to be consistent with CART timescales, for the computation of the residence time, particles are discarded once they have reached an open boundary, e.g. estuarine head or an open boundary in coastal waters (de Brauwere et al., 2011; de Brye et al., 2012). The arithmetic mean of the individual residence times, φ, was computed as the time necessary for particles to exit the domain (ω) for the first time. As for the exposure time, the particles are assumed to immediately bounce back into the domain only at estuarine heads. This simplifying hypothesis is unlikely to entail any major error, since a particle crossing the upstream estuarine boundary in the upstream direction (because of diffusive processes) will most likely return into the estuary after a relatively small time under the influence of the river flow, e.g., the St. Johans River in Florida, which experiences backflows over significant durations (Hendrickson et al., 2003).

Results from residence and exposure times were used to estimate the return coefficient distribution. The residence and exposure times may vary according to the time of release, such as during neap/spring tides or high/low tides, and this would also affect the return coefficient. This notwithstanding, results of exposure and residence times must be calculated for the same conditions when computing the return coefficient, i.e. $r = (\Theta - \varphi)/\Theta$.

2.5. The modified LOICZ analytical model

The modified LOICZ model of Andutta et al. (2014) applies the salinity balance proposed by Fischer et al. (1979) into the original formulation of the LOICZ. This water renewal timescale model has been shown to be sensitive to changes to some of its free parameters (e.g. river flow and salinity grandient). We expect that the estimates of the timescales from our numerical results would fit within the ranges derived from the LOICZ model. Details of its derivation are provided in Andutta et al. (2014); however we provide the simplified relation for water renewal timescale.

$$\frac{1}{T_P} = \frac{1}{T_1} + \frac{1}{T_2}, \tag{4}$$

where $T_1 = L/U$ and $T_2 = L^2/K$ are the advective and dispersive timescales, respectively. L, U, K and T_p are respectively the selected estuarine segment length, the flow speed, the characteristic value of the longitudinal diffusivity and the water renewal timescale. This expression may be re-written in terms of the dimensionless Péclet number $Pe = ULK^{-1}$, the ratio $P_e = T_2/T_1$ of the dispersive to the advective timescale. Similarly, this number provides a comparison of contributions from advective and dispersive processes to transport timescales, yielding

$$T_P = \frac{\mathrm{VP_e}}{Q_R(1 + P_e)}. \tag{5}$$

Where V and Q_R denote the estuarine volume and river discharge, respectively. The contribution of advection to the total water renewal timescale T_P, θ $(0 \le \theta \le 1)$, is given by

$$\theta = T_P/T_I = Q_R/(Q_R + Q_D), \tag{6}$$

where Q_D is the discharge. Eqs. (4) and (6) were used to generate the advective-dispersive diagram (shown later), whose results will be compared to the numerical results.

2.6. The CART analytical model

As previously mentioned, in the framework of CART, the TTS that may be used to calculate water renewal rates can be obtained at any time and position as the solution of partial differential equations (Deleersnijder et al., 2006; de Brye et al., 2012; Andutta et al., 2014). For instance, residence time and exposure time were estimated using calibrated/validated numerical simulations for the Scheldt Estuary (de Brauwere et al., 2011; de Brye et al., 2012). As an easy acceptable method, analytical solutions may provide results that are representative of real situations (e.g. CART and LOICZ). The idealised CART timescales were used to obtain the exact analytical solution of the so called return coefficient for the ESCP. Different values of the Péclet number were considered, in order to assess the axial variation of return coefficient values. The advective timescale, $T_1 = V/Q_R$, and a dispersive timescale, $T_2 = P_E V/Q_R$, are defined taking into consideration the estuarine volume V. Andutta et al. (2014) provides a detailed description depicting an idealised channel for the time scales.

Consider an estuarine channel $(-\infty < x < \infty)$ with a constant

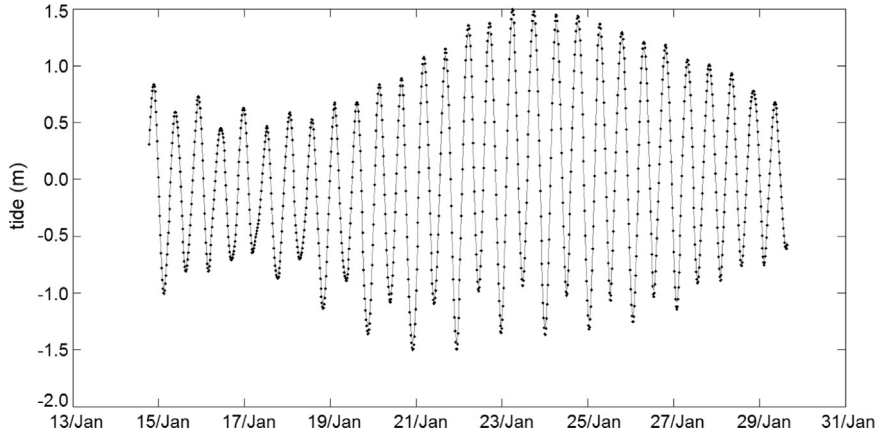

Fig. 5. Modelled water column (m) at station A compared to measured tides, from 14th to 29th of January 2008. Dots denote observations, and line denotes model result.

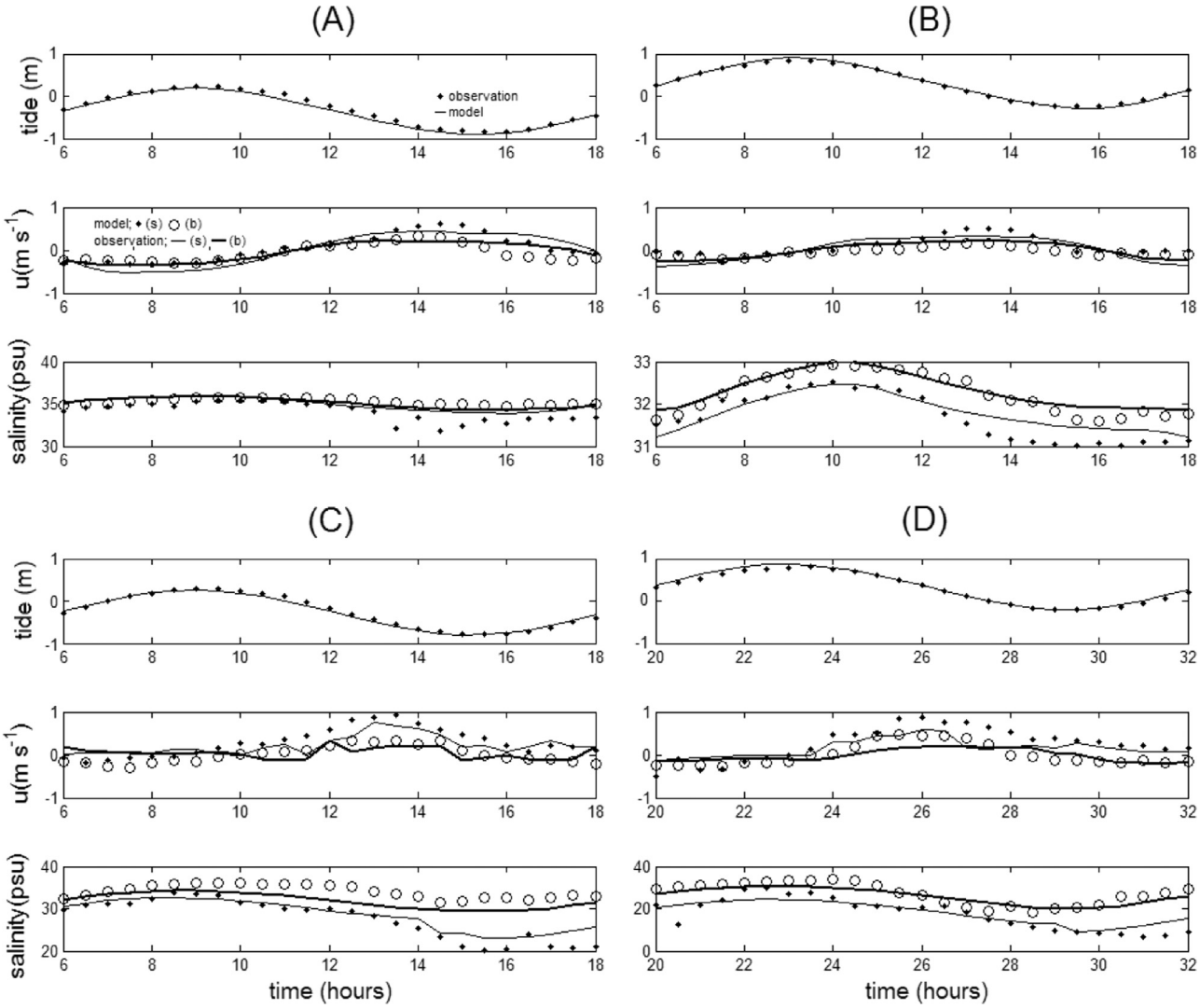

Fig. 6. Modelled tide (m), axial channel velocity u (m s^{-1}) and salinity () compared to measured time series at stations A, B, C, and D, during neap tides. Measurements and simulation represented at the surface and bottom layers. Skill values are synthesised in Table 4.

Table 4.
Results of the validation using the Skill method from Wilmott (1981).

Parameter	Site A (Skill)	Site B (Skill)	Site C (Skill)	Site D (Skill)
Tidal height (neap)	0.99	1	0.99	0.99
Tidal height (spring)	1	0.99	1	0.98
Velocity (neap)	0.68	0.65	0.62	0.65
Velocity (spring)	0.77	0.93	0.84	0.88
Salinity (neap)	0.85	0.80	0.73	0.78
Salinity (spring)	0.97	0.85	0.83	0.93
Parameter	Site A (Skill)		Site B (Skill)	
Velocity (14–26th Jan 2008)	0.72		0.78	

cross-sectional area A, and a flow under steady-state. The volumetric flow rate is denoted as Q_R. The downstream and upstream boundaries of our idealised estuary are located at $x = L_0$ and $x = L_1$, respectively. The estuarine length is $L = L_0 - L_1$, and thus the volume is $V = AL$. The water velocity is then $U = Q_R/A = LQ_R/V$. For the abovementioned conditions, the residence time satisfies the adjoint of the classical passive tracer transport equation (Delhez et al., 2004; Andutta et al., 2014), i.e.

$$\frac{d}{dx}\left(AK\frac{d\varphi}{dx} + Q_R\varphi\right) = -A \tag{7}$$

where, x, denotes the particle position. The solution for the equation needs to satisfy the upstream and downstream boundary conditions,

$$\varphi(L_1) = 0 = \varphi(L_0). \tag{8}$$

It represents the average time required by particles initially located in the interval $[x, x + \delta x]$ (with $\delta x \to 0$) to reach one of the open boundaries. The solution is then easily derived:

$$\varphi(x) = \frac{V}{Q_R}\left(1 - \frac{\xi}{L}\right) + \frac{V}{Q_R}\left(\frac{e^{-Pe} - e^{-Pe\cdot\xi/L}}{1 - e^{-Pe}}\right) \tag{9}$$

where $\xi = x - L_1$.

The exposure time was also derived (Andutta et al., 2014), and is defined in the domain of interest and its surrounding environment.

$$-\infty \le x \le L_1\colon \Theta(x) = \frac{V}{Q_R} \tag{10a}$$

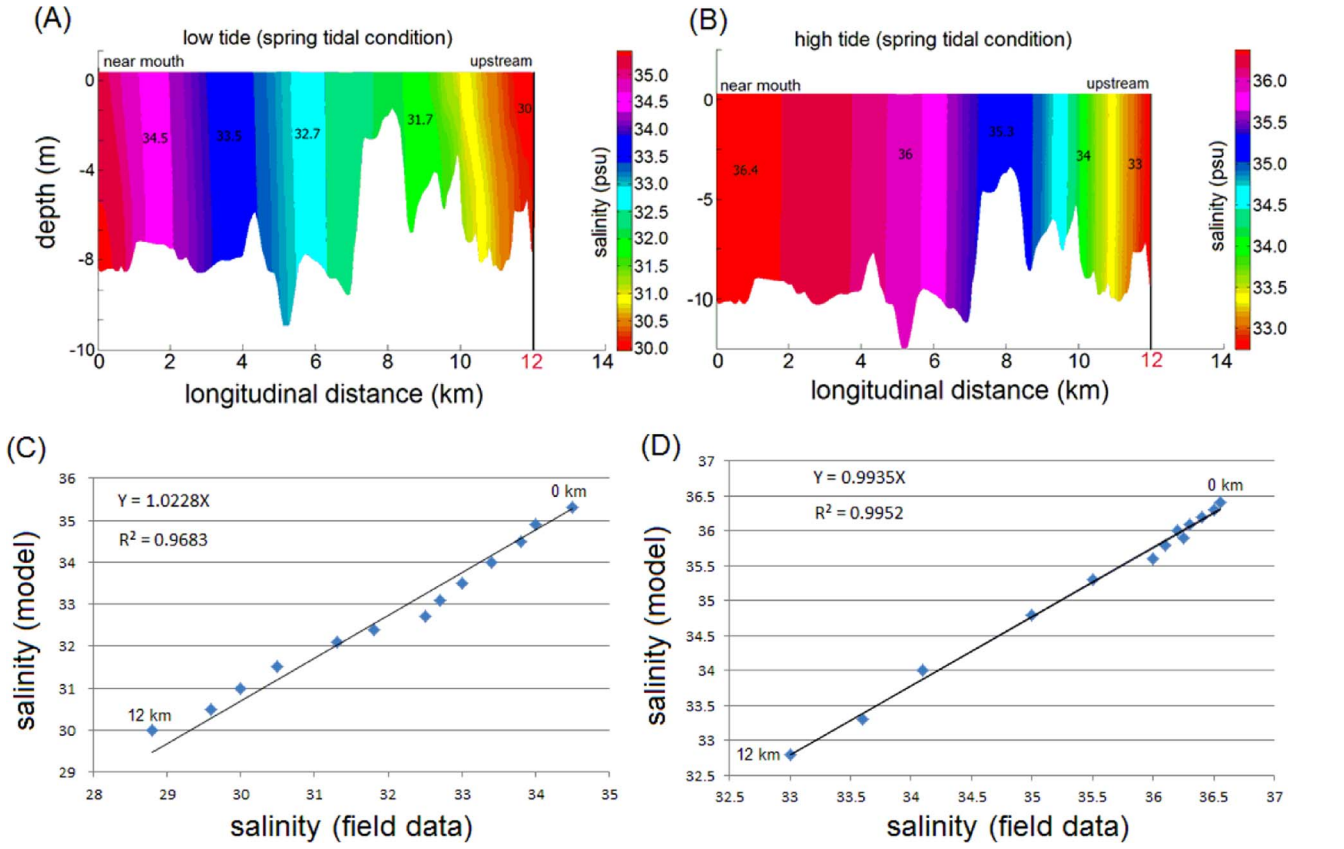

Fig. 7. Axial distribution of salinity () in the Caravelas Estuary in spring tidal conditions, at low (A) and high (B) tide. Correlation of axial distribution of the mean water column salinity between model and observation at low (C) and high (D) tide in spring tide, where Y and X denote model results and measurement, respectively. First dot on left denotes position at estuarine mouth (0 km), while lat dot denotes a position 12 km further upstream, the increment of 1 km is applied from first to last dot. Observations obtained from Schettini and Miranda (2010).

$$L_1 \le x \le L_0:\ \Theta(x) = \frac{V}{Q_R}\left(1 - \frac{\xi}{L}\right) + \frac{V}{Q_R}\left(\frac{1 - e^{-Pe\cdot\xi/L}}{Pe}\right) \tag{10b}$$

$$L_0 \le x < \infty:\ \Theta(x) = \frac{V}{Q_R}\left(\frac{e^{-Pe} - 1}{P_e} e^{-Pe\cdot\xi/L}\right) \tag{10c}$$

From Eq. (9) and (10), which are valid within the upstream and downstream open boundaries, the return coefficient is:

$$r = \frac{\Theta(x) - \varphi(x)}{\Theta(x)} = \frac{\left(\frac{1 - e^{-Pe\cdot\xi/L}}{Pe}\right) - \left(\frac{e^{-Pe} - e^{-Pe\cdot\xi/L}}{1 - e^{-Pe}}\right)}{\left(1 - \frac{\xi}{L}\right) + \left(\frac{1 - e^{-Pe\cdot\xi/L}}{Pe}\right)} \tag{11}$$

Note that r is bounded by [0,1], as mentioned before.

In principle, the residence time and the exposure time can be obtained by solving classical passive transport equations. However, to do so, time- and position-dependent concentrations must first be obtained and, then, time and space integral must be performed to derive the relevant timescales. This is not straightforward, even for highly idealised flows. This is why it is preferable to have recourse to the adjoint method established by Delhez et al. (2004), which requires the solution of simpler differential problems to be determined: in the present case, only ordinary differential equations are to be dealt with rather than partial differential ones. The disadvantage of this approach is that the theoretical underpinning of an adjoint model sometimes appears elusive, which is probably the reason why Errico (1997) wrote a general, enlightening paper on this matter, explaining the nature and purpose of adjoint models.

3. Results and discussion

3.1. Model calibration of salinity, velocity and tides

We carried out a sensitivity analysis considering different values for the horizontal diffusion coefficient k_h using Eq. 2. These adjustments of factor f for the horizontal diffusivity based on the grid size allowed us to obtain a proper representation of the salinity field and its time variability.

The mean Skill parameters for the simulation are shown in Table 3 for different values of factor f, which was discribed with Eq. (2). The comparison of sea-level oscillation over a tidal modulation period, from the 14th to the 29th of January 2008, showed good skill values for locations A (Fig. 5) and C (not shown), and the Skill parameter for tides was calculated to be over 0.97 for both locations, i.e. A and C. The comparison of tides, velocity, and salinity showed good skill values during spring tides (not shown), and reasonable values during neap tides (Fig. 6).

The Skill parameter for the water column height variation in time was calculated to be over 0.98 for all the sites under neap and spring tides (Table 4), and the tidal ranges were ~1.0 m and ~2.5 m for neap and spring tides, respectively. Observations have shown that the tidal phase between sites A (Caravelas mouth) and C (Peruípe mouth) is almost the same. The similarity of their phases indicates that tides propagate mainly perpendicular to the coast line in this region, a result which is in close agreement with observations previously reported by Lessa and Cirano (2006).

For the modelled velocity validation, good results (Skill from 0.77 to 0.93) were obtained in spring tides in the estuaries of Caravelas (sites A and B) and Nova Viçosa (sites C and D). For neap

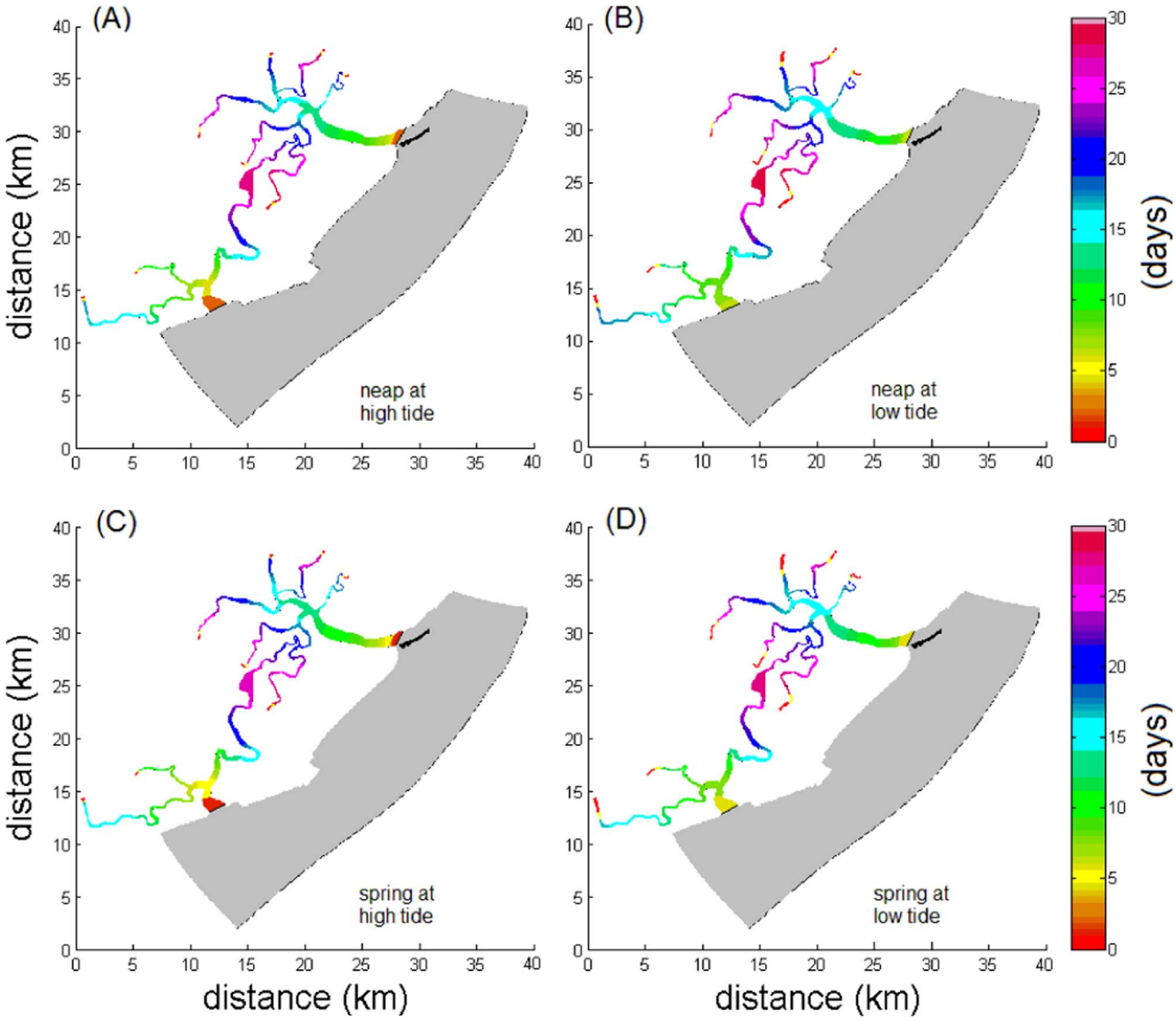

Fig. 8. Verically averaged residence time spatial distribution (ϕ), for scenarios S_1 (A), S_2 (B), S_3 (B) and S_4 (C). Colored bar indicates the timescales in days.

tides due to small differences on tidal asymmetry, the Skill was lower, at ~ 0.6.

The model agreed well with observations of maximum ebb and flood currents at site A. The model also properly simulated the velocity profiles for sites B, C, and D. Therefore, the description of maximum ebb and flood currents from in-situ data also apply to the model simulations. At site B there were maximum speeds of $\sim 0.5\ m\ s^{-1}$ and $1.0\ m\ s^{-1}$ (ebb events), and $\sim -0.3\ m\ s^{-1}$ and $\sim -0.6\ m\ s^{-1}$ (flood events), during neap and spring tides, respectively. For site A the vertical shear of the velocity was negligible in flood and ebb conditions, while for site B there was a small vertical shear of the horizontal velocity during ebb events. During flood events, the water velocity was homogenous over the water column. In addition, a residual velocity of $\sim 0.05\ m\ s^{-1}$ was calculated at site B, indicating a residual circulation from Nova Viçosa towards the Caravelas River. Site A had a residual current of $\sim 0.06\ m\ s^{-1}$, indicating a small discharge from the Cupído and Jaburuna Rivers. At sites C and D, located in the Peruípe River, the downstream velocities showed more intensity than observed in the Caravelas Channel. For site C the downstream velocities varied from $\sim -0.9\ m\ s^{-1}$ to $\sim -1.5\ m\ s^{-1}$, for neap and spring tides, respectively. During flood events, the velocities were $\sim -0.3\ m\ s^{-1}$ and $\sim -0.7\ m\ s^{-1}$, for neap and spring tides, respectively. At site D the maximum downstream velocities were only $\sim 0.7\ m\ s^{-1}$ and $\sim 1.0\ m\ s^{-1}$ at neap and spring tides, and upstream velocities were $\sim -0.3\ m\ s^{-1}$ and $\sim -0.4\ m\ s^{-1}$. The residual velocities at sites C and D, which have values of $\sim 0.10\ m\ s^{-1}$ to $\sim 0.15\ m\ s^{-1}$, indicate a higher advective contribution from the Peruípe River compared with the Caravelas estuary.

In addition to the tides and the velocity field, the model simulated the temporal variation of the salinity well for all sites (A, B, C, and D). During spring tides the calculated Skill values were over 0.83, while for neap tides they were over 0.73 (Table 4). At the Caravelas estuarine channel, ~3 km near the mouth (site A), during low tide, salinity was observed in intervals of ~34.5 psu to ~35.0 psu and ~34.0 psu to ~34.5 psu for the observational and theoretical results, respectively. About 6 km away from the mouth we obtained a good agreement for the salinity, with ~32.0 psu and ~32.5 psu for observation and simulation, respectively. In the vicinity of the interconnection with Cupído and Jaburuna Rivers (site B), which is about 12 km upstream from the mouth, the salinity decreased to ~30.0 psu and ~28.5 psu for the observational and calculated results, respectively. At high tide, near the

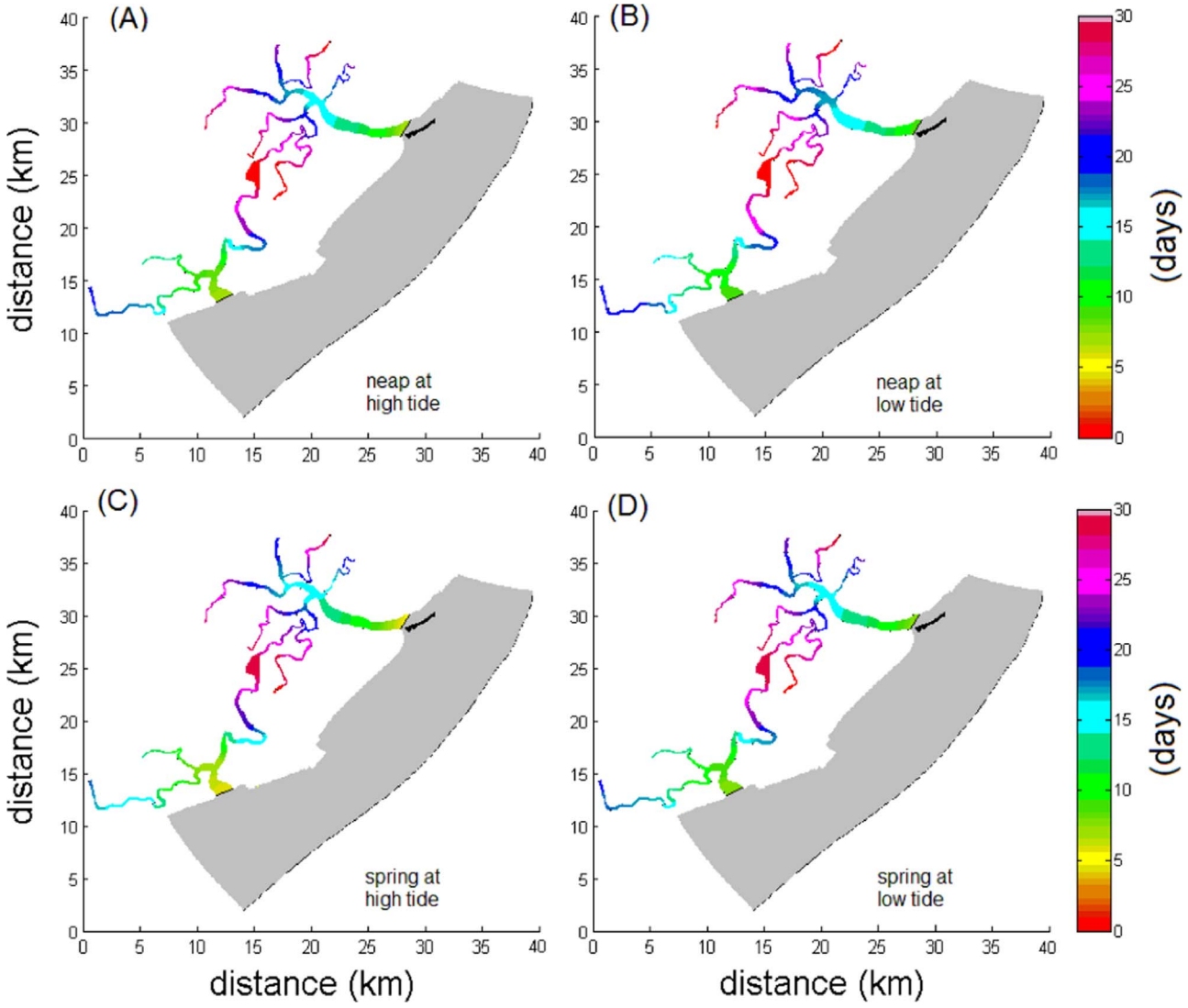

Fig. 9. Vertically averaged exposure time spatial distribution (Θ), for scenarios S_1 (A), S_2 (B), S_3 (B) and S_4 (C). Colored bar indicates the timescales in days.

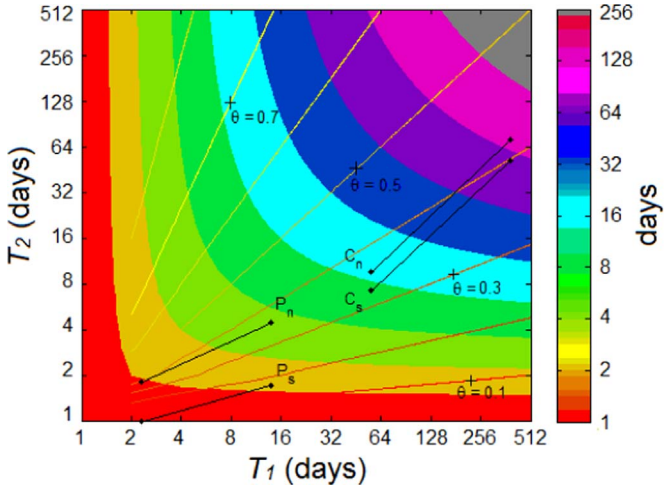

Fig. 10. The position of Caravelas (CA) and Peruípe (P) estuaries on the advection-diffusion diagram to indicate the relative contribution to the water renewal T_P by the advective (T_1) and dispersive (T_2) timescales using a logarithmic scale. Subscript (n) and (s) indicate neap and spring tide conditions.

mouth (site A) and at a distance of 6 km from the mouth, the salinity was ~36.5 psu and ~36.0 psu, respectively, for both simulation and field measurements. In the upper reaches of the estuary, near the junction of the rivers, Cupído and Jaburuna (~12 km from the mouth), a close agreement between simulated and observed salinity values (~33.0 psu) was obtained at high tide. Along the Peruípe River estuary at neap tides, the surface salinities vary in the range of 20.0 psu to 34.0 psu at the surface, and 32.5 psu to 36.0 psu near the bottom. The region of Nova Viçosa has more vertical stratification of the salinity than at sites A and B in the Caravelas River. This is due to Peruípe River's larger freshwater discharge. The observed value of ~36.0 psu near the bottom is characteristic of the Tropical Water Mass, which was already reported to enter this estuarine system (Schettini et al., 2010). During spring tides the vertical mixing causes the erosion of the halocline, and thus decreases vertical stratification. This results in a smaller vertical variation of 31.0 psu to 36.0 psu from the surface to the bottom.

A comparison of the axial distribution of salinity was made for the Caravelas River (Fig. 7A and B). For the first 12 km along the estuarine channel, results from simulations were compared to observations made by Schettini and Miranda (2010). The measurements were obtained on the 10th of April 2001 during spring tides. Although the field data are likely to be from different

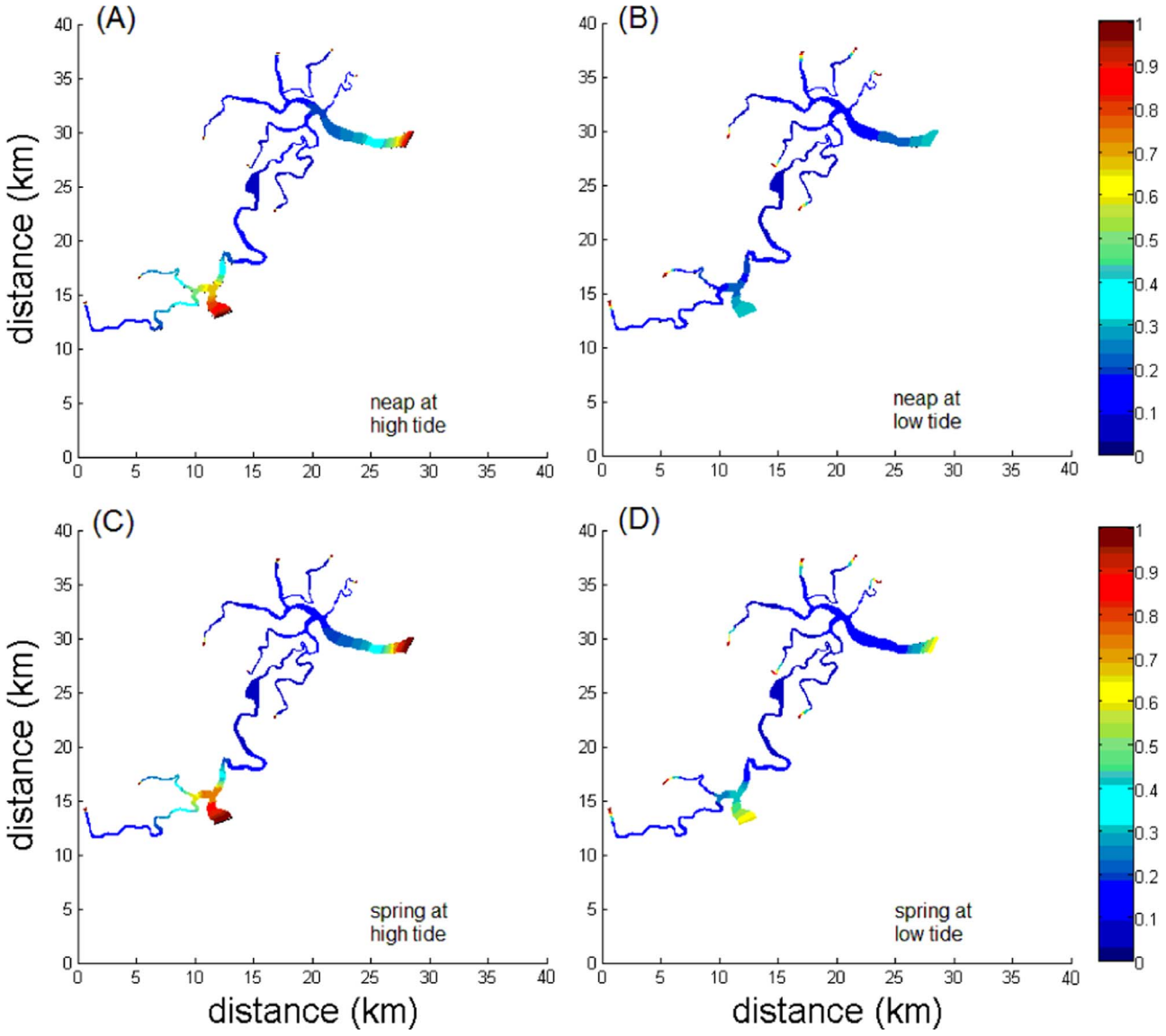

Fig. 11. Return coefficient spatial distribution (r), for scenarios S_1 (A), S_2 (B), S_3 (B) and S_4 (C). Colored bar indicates the timescales in days.

conditions of river flow, the simulation showed a good correlation of the axial distribution of the salinity in the Caravelas River (See Fig. 7C and D), with values of $R^2 \sim 0.97$ and $R^2 \sim 0.99$ for low and high tides respectively. This indicates that the model has well represented the mixing processes in the Caravelas Estuary. During low tide (Fig. 7A and C), a good agreement is found near the mouth, with salinity values of ~35.2 psu and ~ 34.5 psu, for the model results and observations, respectively. At nearly 6 km upstream, there is still a good agreement ($R^2 \sim 0.99$) with the salinity values of ~33 psu (model), and ~32 psu (observation). Further upstream and near the inter-conection between the Cupído and Jaburuna rivers (i.e. ~12 km upstream), the agreement is slightly poorer with the salinity values of ~30 psu (model) and ~29 psu (observation). At high tide (Fig. 7B and D), the model predicted the longitudinal salinity variations well along the Caravelas Channel. The salinity values near the mouth were ~36.4 psu (model and observation), and reduced to ~36 psu 6 km further upstream. Moreover, during high tides the agreement was also good near the channel between the Cupído and Jaburuna rivers with salinity of ~33 psu.

3.2. Results of the residence time, the exposure time and the return coefficient

The transport timescales, namely residence time (φ), exposure time (Θ), and the return coefficient (r), were estimated for the Caravelas and Peruípe estuarine channels with simulation under different scenarios, i.e. S_1–S_4 (Figs. 8 and 9).

For scenarios S_1 and S_3 (Fig. 8), the residence time along the Caravelas Channel, from the mouth to 12 km upstream, was found to vary from 0 to ~15.0 days. The inflow boundaries of the Cupído and Jaburuna rivers were found to have residence times of ~27 and ~22 days, respectively. For the Peruípe Channel the residence times ranged from 0 to ~7.4 days, from the mouth to 5 km upstream, with a maximum value of ~18 days at the inflow boundary of the Peruípe Estuary.

The residence time estimated at ~6 km further upstream in the Caravelas Estuary ($\varphi = 11.7$ days) is almost three times larger than the residence time calculated for the same distance along the Peruípe Estuary ($\varphi < 4.4$ days). The difference between results in the Caravelas and the Peruípe estuaries is due to the larger velocity

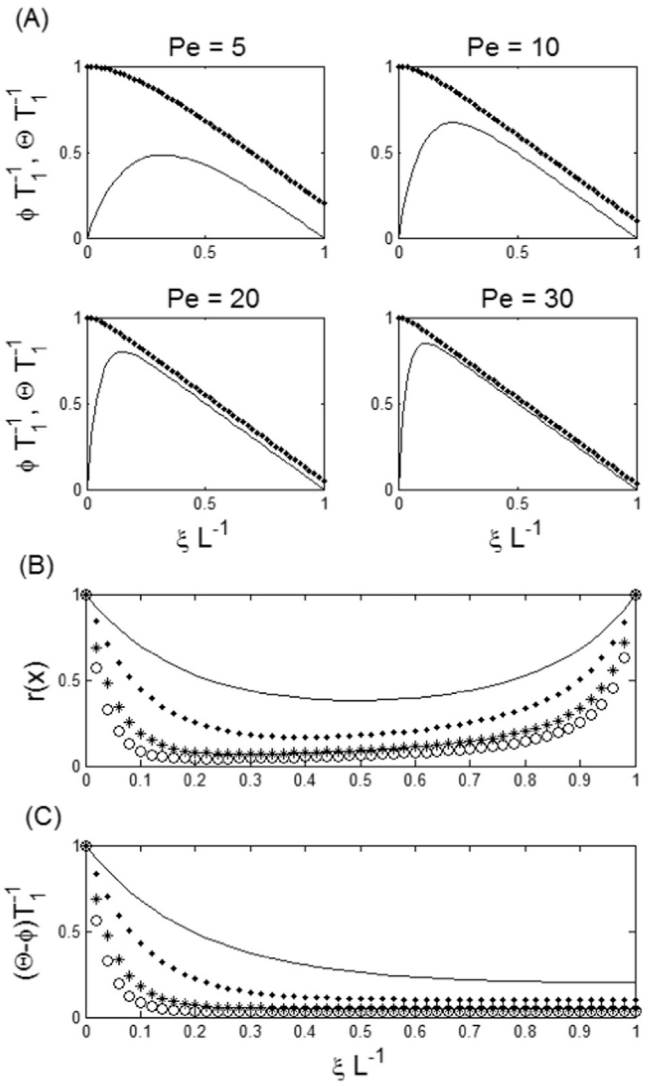

Fig. 12. (A) Representation of the exposure time Θ (dots) and residence time φ (line) as a function of the distance x from the upstream boundary of the domain. (B) Return coefficient and (C) and the difference between the exposure and residence time ($\Theta - \varphi$) calculated for different values of Peclet number, Pe=5 (line), Pe=10 (dot), Pe=20 (star), and Pe=30 (circle). The timescales are normalised by means of the advective timescale T_1.

contribution in the Peruípe Estuary.

Comparing scenarios S_1 and S_3, the residence time was found to be slightly lower for S_3 (c.a. a few hours) and this difference is due to increased diffusive contribution during stronger spring tidal conditions. In contrast to scenarios S_1 and S_3, the simulations considering scenarios S_2 and S_4 yielded an increased residence time. This increase was maximum near the estuarine mouths ($\sim$5 days), and observed to reduce in the upstream direction (few hours). The increase in residence time for particles released in slack water of low tide is caused by tidal excursion from reversing currents (i.e. flood currents). These results reflect and add value to recent simulations by de Brye et al. (2012) for the Scheldt Estuary (in Belgium and the Netherlands), whose results showed larger residence time values for particles released at slack water of low tides than for high tides (difference of a few days).

The virtual Lagrangian particles showed that a negligible number of particles crossed the connecting channel between the Caravelas (ω_1) and Peruípe Estuaries (ω_2), which indicates that this relatively narrow and shallow interconnection channel allows little exchange of water properties between these estuaries. Moreover, the residence time is observed to be larger within the enlargement of the interconnecting channel between these two estuaries. Schettini and Miranda (2010) and Schettini et al. (2013) have addressed the importance of the interconnection channel between Caravelas and Peruípe, and found that sediment deposited near the Caravelas mouth was both inner shelf local resuspension and upstream transport, or sourced from the Peruípe River via the interconnection channel.

Exposure time results showed that particles re-entered the system for up to two days (Fig. 9). Note that the difference between the exposure time and the residence time ($\Theta - \varphi$) showed little spatial variation for scenarios S_1 and S_3.

The spatially averaged difference between exposure and residence times ($\Theta - \varphi$) are calculated in days, and its respective RMSE to be $\sim 1.98 \pm 0.06$ for S_1, $\sim 1.87 \pm 0.12$ for S_2, $\sim 1.92 \pm 0.07$ for S_3, $\sim 2.19 \pm 0.08$ for S_4. These results strongly suggest that ($\Theta - \varphi \sim$ const.) for the ESCP under the four different scenarios considered. The results also suggest that t_3–t_2 varies little away from the open boundaries, so particles deployed at different times and locations in the estuary re-enter for similar lengths of time, assuming the circulation in coastal waters does not considerably change over time due to additional forcing, e.g. sudden alongshore wind driven currents.

Eq. (5) was used to estimate the range of water renewal timescales for the Caravelas and Peruípe estuaries using the parameters given in the appendices of Andutta et al. (2014), see Fig. 10. The straight line labelled θ (lowercase) indicate the relative advective contribution to water renewal, where $0 \leq \theta \leq 1$. The line at $\theta = 0.5$ separates the areas where transport is dominated by advection (diagram upper zone, $\theta > 0.5$) and dispersion (diagram lower zone, $\theta < 0.5$).

The Caravelas and Peruípe estuaries have mean depths of $\sim$6.5 and $\sim$7.5 m, respectively, and the maximum and minimum tidal ranges in these estuaries are $\sim$2.5 and $\sim$0.5 m. According to Andutta et al. (2013), these tidal ranges combined with the relatively the small depths result in a high rate of change of the potential energy ($\sim 6.1\ \mathrm{J\,m^{-3}\,s^{-1}}$), which contributes towards large dispersion. It is valid to compare these results to the Sheldt Estuary, where tidal oscillation is typically 4–5 m along the first $\sim$100 km, and where the mean water depth is $\sim$10 m. Tidal range in the Sheldt can reach $\sim$7 m, which is about 45% of the mean water depth value for the first $\sim$25 km near the estuarine mouth (Soetaert and Herman, 1995; de Brye et al., 2012), and this system is classified as well-mixed due to dispersion prevailing over advection. The numerical results for the ESCP fit within the timescale ranges estimated using the simple LOICZ method.

The return coefficient cannot be calculated using the modified LOICZ model. However, it was computed numerically and compared to the non-dimensional solution obtained using CART. The return coefficient converges to one at the estuarine mouths and near estuarine heads (Fig. 11, for all scenarios S_1–S_4 and Fig. 12B). However, this is only a direct consequence of the definition of the residence time, which converges to zero at the entrance, and thus the return coefficient will always increase towards unity. r was observed to be smaller upstream, because the ratio $(\Theta - \varphi)/\Theta$ is likely to decrease. It can be noticed that the axial variation of the return coefficient is similar for both CART solution and numerical approach (Figs. 11 and 12C). The return coefficient calculated from CART and from numerical simulations is observed to increase towards the upstream boundary. This increase towards the estuarine head is due to the boundary condition assumed in the analytical and numerical solutions, where particles do not re-enter the domain after crossing the estuarine head, although in a real estuary water particles would re-enter through the estuarine head due to river flow conditions.

Fig. 12A shows results of the residence and exposure time and

return coefficient for a range of values of the Péclet number. High values of the Péclet number yield a boundary layer in the vicinity of the upstream location.

The greater the relative importance of advection, the less likely it is that dispersion will cause a water particle to hit the upstream boundary of the domain ($x=L_0$). In accordance with their definitions, the exposure time is larger than the residence time for any location in the domain ($L_1\ \xi/LL_0$). These idealised results of the return coefficient were used to access results obtained from our numerical simulations.

In the illustration shown in Fig. 11A, the ratio is simply the difference between times t_3 and t_2. Evidently this is a simple case where the particle is assumed to have re-entered the domain only once.

Particles are expected to first cross the estuarine mouth during ebb currents, which would be alternating with flood currents and dispersive processes. Therefore, we could presume that Lagrangian particles would have a time window of ~6.5 h to cross the entrance (for semi-diurnal tidal estuaries), and this time window would then close for ~ 6.5 h (the period of flood currents).

Our simulations were for relatively calm weather conditions, which were predominant over the region, c.a. wind speeds in the range 1–4 m s^{-1} (wind from NE). Andutta et al. (2013) showed that wind conditions did not affect the water circulation in this estuarine system in January 2008. However, for stronger wind conditions the results would not be the same. Evidently alongshore wind-driven currents would reduce the difference between the exposure time and the residence time, and the return coefficient would thus decrease towards zero. This is because alongshore currents inhibit the propensity of particles to re-enter the estuarine system. The alongshore shelf currents are observed to be driven by the N-S migration of the South Atlantic High between summer and winter. South-southwestward alongshore currents occur between October and January, while stronger north-northeastward alongshore currents are observed during the fall and winter months (Lessa and Cirano, 2006).

4. Conclusions

4.1. Overall goal

This study provides the first estimates of the residence time, exposure time and the return coefficient for the Caravelas and Peruípe estuaries and might be a reference for future studies related to the control of pollutants and sediment transport. These transport timescales were estimated using a Lagrangian model only as a tool, and this model has been properly calibrated and validated using field data.

4.2. Specific conclusions

- Achievements regarding goals (1 and 2)

The residence time for particles released far upstream in the Caravelas Estuary was found to be nearly 3 weeks for particles, regardless of whether they are released at high or low tide, and is driven by tidal dispersion combined with the discharge from the Cupído and Jaburuna Rivers (typical range of 4–9 $m^3\ s^{-1}$). These results are consistent with previous estimates derived from simple analytical solutions (Andutta et al., 2014), see Fig. 10. For the Peruípe Estuary, our estimates of the residence time were for less than one week, due to the tidal dispersion combined with the larger river input from the Peruípe River (typical range of 20–70 $m^3\ s^{-1}$).

The transport timescales (exposure and residence times) were found to be quite similar for particles released in high tide under spring and neap tidal conditions, thus confirming previous estimations made for the Scheldt Estuary (de Brye et al., 2012). In contrast, the transport timescales were shown to be more sensitive to tidal-phase release time (i.e. high or low tides) in this estuarine system. Similar observations were made for the Scheldt Estuary (de Brauwere et al., 2011), in which there was a difference of days for results of residence time using particles released at high and low tides. This suggests that tidal-phase release time for a meso-tidal shallow estuary forced by low-moderate river discharge conditions is important for quantification of TTS, especially for water particles near mouths where larger tidal excursions are expected compared to locations further upstream, and since their initial movement would be upstream/downstream if released during low/high tide, respectively.

The Lagrangian simulation also showed that the narrow and shallow inter-connecting channel between the Peruípe and Caravelas estuaries allows little water exchange between the two estuaries, and only a few particles were capable of crossing the inter-connection passage with prevailing direction from the Peruípe to the Caravelas, in agreement with Schettini et al. (2013). Therefore, both exposure time and residence time were large at that location, and the exchange of water properties is likely to happen through alongshore currents at inner coastal areas.

- Achievements regarding goal (3)

Similarly to the exposure and residence times, the return coefficient was shown to be more sensitive to tidal phase (high and low tide), than to neap and spring tidal conditions. It may be summarized as follows: (1) the return coefficient is larger for particles released at high tide than at low tide; (2) the return coefficient is larger for particles released during spring tides than during neap tides.

For these two estuaries the exposure time was higher than the residence time in all simulations, thus showing that water may return to the system after having first crossed the mouth. The propensity of this water to return to the estuary was quantified using the return coefficient, which depends on the difference between the exposure and residence times, and thus also on the residual circulation due to river discharge, as well as the circulation in coastal waters. For instance, swift longshore currents decrease the difference between the exposure and residence times, and therefore reduce the return coefficient. The wind conditions over our measurement period were characteristic of calm weather, c.a. a few m s^{-1} (see Fig. 4), and different scenarios may produce different results for the transport timescales, for instance under stronger north-northeastward alongshore currents which are often observed during the fall and winter months Lessa and Cirano (2006). Due to its definition, the return coefficient is predicted to be larger at the estuarine mouths, because the residence time tends to zero (see Eq. (1)). Our results have additionally shown that for our scenarios the difference between exposure and residence times ($\Theta - \varphi$) is nearly constant within our domain. This can also be observed from our analytical solution (Fig. 12C).

Acknowledgements

We acknowledge the Conselho Nacional de Desenvolvimento Científico e Tecnológico (CNPq), and the CNPq grant 420219/2005-6 to Eurico Cabral de Oliveira, and the CNPq fellowships (Procs. LBM-302069/2004-6, CAFS-306217/2007-4 and ES-308303/2006-7). We also acknowledge the assistance in the field work from

Carlos A. F. Schettini, Eduardo Siegle, Mario Pereira, Piero L. F. Mazzini, Vitor M. Izumi, and the collaboration of other graduate students and technicians of the Dept. of Physical, Chemistry and Geology of IO-USP, PPGGeo/UFRGS and UFRN. Eric Deleersnijder is an honorary Research Associate with the Belgian Fund for Scientific Research (F.R.S.-FNRS).

Appendix A. Supplementary material

Supplementary data associated with this article can be found in the online version at http://dx.doi.org/10.1016/j.csr.2016.05.006.

References

Andutta, F.P., Ridd, P.V., Deleersnijder, E., Prandle, D., 2014. Using field data for estimating estuarine water transport timescales and the associated return coefficient. Progress. Oceanogr. 120, 139–153. http://dx.doi.org/10.1016/j.pocean.2013.08.009.

Andutta, F.P., Miranda, L., Schettini, C.A.F., Siegle, E., da Silva, M.P., Izumi, V.M., Chagas, F.M., 2013. Temporal variations of Temperature, Salinity and circulation in the Peruípe River Estuary (Nova Viçosa, BA). Cont. Shelf Res. 70, 36–45. http://dx.doi.org/10.1016/j.csr.2013.03.013.

Andutta, F.P., 2011. The Estuarine System of the Caravelas and Peruípe Rivers (Bahia): Observations, Simulations, Residence Time, and Advective and Diffusive Processes (Ph.D. thesis). IO-USP, Oceanography Institute of the University of São Paulo 121 pp.

Bolin, B., Rodhe, H., 1973. A note on the concepts of age distribution and transit time in natural reservoirs. Tellus 25 (1), 58–62.

Davies, J.H., 1974. A Morphogenic Approach of World Shorelines. Z. Geomorphology 8, 127–142.

Defant, A., 1960. Physical Oceanography. 2. Pergamon Press, New York, p. 598.

Deleersnijder, E., Beckers, J.-M., Delhez, E.J.M., 2006. On the behaviour of the residence time at the bottom of the mixed layer. Environ. Fluid Mech. 6, 541–547.

Delft Hydraulics, 2008. Delft-3D Flow Manual. Delft Hydraulics, Delft, Holanda, p. 674.

Delhez, E.J.M., Heemink, A.W., Deleersnijder, E., 2004. Residence time in a semi-enclosed domain from the solution of an adjoint problem. Estuar. Coast. Shelf Sci. 61, 691–702.

Delhez, E.J.M., de Brye, B., de Brauwere, A., Deleersnijder, E., 2014. Residence time vs influence time. J. Mar. Syst. 132, 185–195. http://dx.doi.org/10.1016/j.jmarsys.2013.12.005.

de Brauwere, A., de Brye, B., Blaise, S., Deleersnijder, E., 2011. Residence time, exposure time and connectivity in the Scheldt Estuary. J. Mar. Syst. 84, 85–95. http://dx.doi.org/10.1016/j.jmarsys.2010.10.001.

de Brye, B., de Brauwere, A., Gourgue, O., Delhez, E.J.M., Deleersnijder, E., 2012. Water renewal timescales in the Scheldt Estuary. J. Mar. Syst. 94, 74–86.

Errico, R.M., 1997. What is an adjoint model? Bull. Am. Meteorol. Soc. 78, 2577–2591.

Fischer, H.B., List, E.Y., Koh, R.C.Y., Imberger, J., Brooks, N.H., 1979. Mixing in Inland and Coastal Waters. Academic Press, New York, p. 483.

Franco, A.S., 2000. Mares: Programa para previsão e analise. Manual, BSP, São Paulo, 36 pp.

Hendrickson, J.C., Lowe, E.F., Dobberfuhl, D., Sucsy, P., Campbell, D., 2003. Characteristics of Accelerated Eutrophication in the Lower St. Johns River Estuary and Recommended Targets to Achieve Water Quality Goals for the Fulfillment TMDL and PLRG Objectives. Department of Water Resources, St. Johns River Water Management District, Palatka, Florida.

Holzer, M., Hall, T.M., 2000. Transit-time and tracer-age distributions in geophysical flows. J. Atmos. Sci. 57, 3539–3558.

Ketchum, B.H., 1951. The exchanges of fresh and salt water in tidal estuaries. J. Mar. Res. 10, 18–38.

Lessa, G.C., Cirano, M., 2006. On the circulation of a coastal channel within the Abrolhos Coral-Reef system-Southern Bahia. Braz. J. Coast. Res. 39, 450–453.

Monsen, N.E., Cloern, J.E., Lucas, L.V., Monismith, S.G., 2002. A comment on the use of flushing time, residence time, and age as transport time scales. Limnol. Oceanogr. 47, 1545–1553.

Okubo, A., 1971. Diffusion diagrams. Deep-Sea Res. 18, 789–802. http://dx.doi.org/10.1016/0011–7471(71)90046–5.

Pereira, M.D., Siegle, E., Miranda, L.B., Shettini, C.A.F., 2010. Hidrodinâmica e transporte de material particulado em suspensão sazonal em um estuário dominado por maré: estuário de Caravelas (BA). Rev. Bras. Geofís. 28 (3), 427–444. http://dx.doi.org/10.1590/S0102-261 × 2010000300008.

Schettini, C.A.F., Pereira, M.D., Siegle, E., Miranda, L.B., Silva, M.P., 2013. Residual fluxes of suspdended sediment in a tidally dominated tropical estuary. Cont. Shelf Res. 70, 27–35. http://dx.doi.org/10.1016/j.csr.2013.03.006.

Schettini, C.A.F., Miranda, L.B., 2010. Circulation and suspended matter transport in a tidally dominated estuary: caravelas estuary, Bahia, Brazil. Rev. Bras. De. Ocean. 58, 1–11. http://dx.doi.org/10.1590/S1679–87592010000100001.

Sheldon, J.E., Alber, M., 2006. The calculation of estuarine turnover times using freshwater fraction and tidal prism models: a critical evaluation. Estuar. Coasts 29, 133–146.

Soetaert, K., Herman, P.M.J., 1995. Estimating estuarine residence times in the Westerschelde (The Neterlands) using a box model with fixed dispersion coefficients. Hydrobiologia 311, 215–224.

Sousa, S.H.M., Amaral, P.G.C., Martins, V., Figueira, R.C.L., Siegle, E., Ferreira, P.A.L., Silva, I.S., Shinagawa, E., Salaroli, A., Schettini, C.A.F., Santa-Cruz, J., Mahiques, M.M., 2012. Environmental evolution of the Caravelas Estuary (Northeastern Brazilian coast, 170S, 390W) based on multiple proxies in a sedimentary record of the last century. J. Coast. Res. 30 (3), 474–486.

Uittenbogaard, R.E., van Kester, J.A.T.M., Stelling, G.S., 1992. Implementation of Three turbulence Models in 3d-TRISULA for Rectangular grids. Tech. Rep Z81. WL J Delft Hydraulics, Delft, The Netherlands.

Wilmott, C.J., 1981. On the validation of models. Phys. Geogr. 2, 184–194.